ARMY RESEARCH LABORATORY

Fluid Structure Interactions for Blast Wave Mitigation

by Wen Peng, Zhaoyan Zhang, George Gogos, and George Gazonas

ARL-RP-0442 **June 2013**

This is a reprint from a paper submitted to the *ASME J. of Applied Mechanics*, Vol. 78, May 2011.

NOTICES

Disclaimers

The findings in this report are not to be construed as an official Department of the Army position unless so designated by other authorized documents.

Citation of manufacturer's or trade names does not constitute an official endorsement or approval of the use thereof.

Destroy this report when it is no longer needed. Do not return it to the originator.

Army Research Laboratory
Aberdeen Proving Ground, MD 21005

ARL-RP-0442 **June 2013**

Fluid Structure Interactions for Blast Wave Mitigation

Wen Peng, Zhaoyan Zhang, and George Gogos
Department of Mechanical Engineering
University of Nebraska-Lincoln
Lincoln, NE 68588

George Gazonas
Weapons and Materials Research Directorate, ARL

This is a reprint from a paper submitted to the *ASME J. of Applied Mechanics*, Vol. 78, May 2011.

REPORT DOCUMENTATION PAGE

Form Approved
OMB No. 0704-0188

1. REPORT DATE *(DD-MM-YYYY)*	2. REPORT TYPE	3. DATES COVERED (From - To)
June 2013	Reprint	

4. TITLE AND SUBTITLE
Fluid Structure Interactions for Blast Wave Mitigation

5a. CONTRACT NUMBER
W911NF-04-2-0011

5b. GRANT NUMBER

5c. PROGRAM ELEMENT NUMBER

6. AUTHOR(S)
Wen Peng, Zhaoyan Zhang, George Gogos, and George Gazonas

5d. PROJECT NUMBER

5e. TASK NUMBER

5f. WORK UNIT NUMBER

7. PERFORMING ORGANIZATION NAME(S) AND ADDRESS(ES)
U.S. Army Research Laboratory
ATTN: RDRL-WMM-B
Aberdeen Proving Ground, MD 21005

8. PERFORMING ORGANIZATION REPORT NUMBER
ARL-RP-0442

9. SPONSORING/MONITORING AGENCY NAME(S) AND ADDRESS(ES)

10. SPONSOR/MONITOR'S ACRONYM(S)

11. SPONSOR/MONITOR'S REPORT NUMBER(S)

12. DISTRIBUTION/AVAILABILITY STATEMENT
Approved for public release; distribution unlimited.

13. SUPPLEMENTARY NOTES
This is a reprint from a paper submitted to the *ASME J. of Applied Mechanics*, Vol. 78, May 2011.

14. ABSTRACT

The dynamic response of a free-standing plate subjected to a blast wave is studied numerically to investigate the effects of fluid-structure interaction (FSI) in blast wave mitigation. Previous work on the FSI between a blast wave and a free-standing plate (Kambouchev, N., et al., 2006, "Nonlinear Compressibility Effects in Fluid-Structure Interaction and Their Implications on the Air-Blast Loading of Structures," J. Appl. Phys., 100(6), p. 063519) has assumed a constant atmospheric pressure at the back of the plate and neglected the resistance caused by the shock wave formation due to the receding motion of the plate. This paper develops an FSI model that includes the resistance caused by the shock wave formation at the back of the plate. The numerical results show that the resistance to the plate motion is especially pronounced for a light plate, and as a result, the previous work overpredicts the mitigation effects of FSI. Therefore, the effects of the interaction between the plate and the shock wave formation at the back of the plate should be considered in blast wave mitigation.

15. SUBJECT TERMS
fluid-structure interaction, blast wave mitigation, shock wave, resistance

16. SECURITY CLASSIFICATION OF:			17. LIMITATION OF ABSTRACT	18. NUMBER OF PAGES	19a. NAME OF RESPONSIBLE PERSON
a. REPORT	b. ABSTRACT	c. THIS PAGE			George Gazonas
Unclassified	Unclassified	Unclassified	UU	16	19b. TELEPHONE NUMBER (*Include area code*) (410) 306-0863

Fluid Structure Interactions for Blast Wave Mitigation

Wen Peng

Zhaoyan Zhang
e-mail: zzhang5@unl.edu

George Gogos

Department of Mechanical Engineering,
University of Nebraska-Lincoln,
Lincoln, NE 68588

George Gazonas
U.S. Army Research Laboratory,
Aberdeen Proving Ground, MD 21005

*The dynamic response of a free-standing plate subjected to a blast wave is studied numerically to investigate the effects of fluid-structure interaction (FSI) in blast wave mitigation. Previous work on the FSI between a blast wave and a free-standing plate (Kambouchev, N., et al., 2006, "Nonlinear Compressibility Effects in Fluid-Structure Interaction and Their Implications on the Air-Blast Loading of Structures," J. Appl. Phys., **100**(6), p. 063519) has assumed a constant atmospheric pressure at the back of the plate and neglected the resistance caused by the shock wave formation due to the receding motion of the plate. This paper develops an FSI model that includes the resistance caused by the shock wave formation at the back of the plate. The numerical results show that the resistance to the plate motion is especially pronounced for a light plate, and as a result, the previous work overpredicts the mitigation effects of FSI. Therefore, the effects of the interaction between the plate and the shock wave formation at the back of the plate should be considered in blast wave mitigation.* [DOI: 10.1115/1.4002758]

Keywords: fluid-structure interaction, blast wave mitigation, shock wave, resistance

1 Introduction

Explosions occur in military conflicts, as well as in various industrial applications, such as the petrochemical, chemical, or nuclear industries. Underwater shock or air blast waves induced by explosions in fluid media can result in injuries to military and civilian personnel, as well as property damage. Hence, our understanding and ability to correctly model complex fluid structure interaction phenomena has important consequences for mitigation of infrastructural damage and human injury. Understanding the FSI between a blast wave and a free-standing plate is a very important step in the development of devices for blast wave mitigation. A blast wave impinging on a free-standing plate will cause the plate to recede. The receding motion of the plate relieves the pressure experienced by the plate and results in a decrease in the impulse transmitted to the plate. Meanwhile, the plate motion induces a shock wave behind the plate, which resists the plate motion. The resistance to the plate motion offsets a fraction of the decrease in pressure experienced by the plate, which is due to the receding motion of the plate. As a result, the impulse transferred to the plate increases due to the induced shock wave. Both the receding motion of the plate and the resistance to the plate should be considered in the investigation of FSI between a blast wave and a free-standing plate.

In recognition of the advantages of FSI in blast wave mitigation, both numerical and experimental efforts have been devoted to this research area during the past decade. Kambouchev et al. [1–3] studied the FSI between a blast wave and a free-standing plate in highly compressible medium, having assumed that a constant atmospheric pressure is applied at the back of the plate. The results show that the impulse transmitted to structures will decrease with the reduction of the plate mass for fixed blast intensity. Kambouchev [4] also studied the interaction of acoustic waves and structures in incompressible media. The acoustic waves are governed by linear wave equations. The effects of incompressible media on both sides of structures were considered, and an analytical solution was derived. Chun et al. [5] investigated the FSI of flexible shelters under blast loading using ANSYS and FLUENT. The results were compared with experimental data. It was found that the blast loading and the structural response cannot be analyzed separately due to the FSI between the flexible structure and the blast loading. Therefore, FSI should be considered when the structural deflection rate can influence the solution of the flow field surrounding the structure. Main and Gazonas [6] studied the influence of mass distribution on the uniaxial crushing of a cellular material sandwiched between solid front and back faces, with air blast loading applied to the front face and the back face unrestrained. An analytical model was developed to investigate the crushing response of the system. FSI effects were treated using the results of Kambouchev et al. [1,2] for air blast loading on solid plates. It was found that the FSI approximation of Kambouchev et al. [1,2] is inappropriate when the mass fraction in the core is large relative to the mass in the front face, particularly when the decay period of the pressure pulse is comparable to the propagation time of the densification front. Espinosa et al. [7] proposed a novel experimental methodology that incorporates FSI to assess the dynamic deformation of structures subjected to underwater impulsive loading.

Related papers studying the blast wave propagation and reflection have also appeared in the literature. Tai et al. [8] discussed blast wave interaction and reflection around closed-ended and open-ended bomb shelters. The reflected shock wave patterns transit from regular reflection to Mach reflection in both bomb shelters under an unsteady situation. Shi et al. [9] simulated the blast wave interaction with a standalone structural column. Parametric studies include the scaled distance of the blast, column stiffness, and column dimension and geometry. The formula to predict the reflected pressure and impulse on the front and on the rear surface of the columns with different dimensions and geometry were derived. Blast wave propagation and reflection has been investigated experimentally. Dewey and McMillin [10] used high speed photogrammetry to investigate the blast wave interaction with ideal and real surfaces. It was observed that a smooth surface induces a stronger Mach stem. Takayama and Sekiquchi [11] studied the interaction of a spherical shock wave with a planar or conical wall. The shock wave was induced by expanding a planar shock wave into free space in a conventional shock tube. When a spherical shock wave encounters a planar or conical wall, a transition from regular to Mach reflection takes place with the incidence angle larger than the critical transition angle. Igra et al. [12] investigated blast wave reflection from wedges experimentally and numerically. A shock tube equipped with a very short driver is

Contributed by the Applied Mechanics Division of ASME for publication in the JOURNAL OF APPLIED MECHANICS. Manuscript received February 11, 2010; final manuscript received September 24, 2010; accepted manuscript posted October 12, 2010; published online February 16, 2011. Assoc. Editor: Vikram Deshpande.

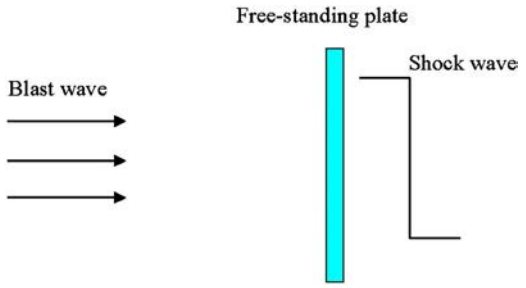

Fig. 1 Schematic of a free-standing plate subjected to a blast wave

employed for the experiments. The reflected wave pattern is similar for the interaction of a blast wave or a shock wave with a wedge when both incident waves have the same initial pressure jump across their fronts, but the resulting pressure field is different.

Previous work [1–3] on the FSI between a blast wave and a free-standing plate in highly compressible medium has neglected the shock wave induced at the back of the plate caused by plate motion. This assumption leads to overprediction of the effectiveness of FSI in blast wave mitigation. In another work [4], the effects of incompressible media on both sides of structures were considered for FSI between acoustic waves and structures. Since the blast wave is a shock wave governed by nonlinear wave equations as opposed to an acoustic wave governed by linear wave equations, their simplification results in conclusions that cannot be readily applied to blast wave mitigation. To accurately model the FSI between a blast wave and a free-standing plate in highly compressible medium, it is necessary to develop a model that includes the shock wave induced by the plate motion. In this paper, a numerical model is developed to simulate the blast wave reflection from a free-standing plate, the plate motion, and the shock wave induced at the back of the plate. The model is validated by comparing results with numerical and analytical results available in the literature for special cases. The numerical results are presented and analyzed in subsequent sections.

2 Mathematical Formulation and Numerical Approach

2.1 Governing Equations. The schematic of the FSI between a blast wave and a free-standing plate is shown in Fig. 1. The plate separates the computational domain into two parts: flow field in front of the plate and flow field at the back of the plate. The flow fields on both sides can be modeled as one-dimensional inviscid compressible flows, which are described by the Euler equations. They can be written in vector form as

$$\frac{\partial U}{\partial t} + \frac{\partial F}{\partial x} = 0 \tag{1}$$

where U is the solution vector, F is the flux vector, t is time, and x is the space coordinate in the flow direction. U and F are given by

$$U = \begin{Bmatrix} \rho \\ \rho u \\ \rho e_t \end{Bmatrix} \quad F = \begin{Bmatrix} \rho u \\ \rho u^2 + p \\ (\rho e_t + p)u \end{Bmatrix}$$

where ρ is the density, p is the pressure, u is the velocity, and e_t is the total energy per unit mass of the compressible flow. The total energy per unit mass is the sum of its internal energy per unit mass, e, and its kinetic energy per unit mass, $u^2/2$. To close the governing equations, it is assumed that the compressible substance obeys calorically perfect ideal gas law given by $p=\rho RT$ and $e=(RT)/(\gamma-1)$, where T is the temperature, R is the gas constant, and γ is the specific heat ratio.

The free-standing plate is treated as a rigid body, and the effects of deformation and stress-wave propagation within the plate are neglected. The free-standing plate obeys Newton's second law of motion

$$\frac{du_p}{dt} = \frac{\Delta p_p}{\rho_p h_p} \tag{2}$$

where u_p is the velocity of the plate, ρ_p is the density of the plate, h_p is the thickness of the plate, and Δp_p is the difference between the reflected pressure in front of the plate and the induced shock wave pressure at the back of the plate.

2.2 Initial and Boundary Conditions. The initial conditions for the flow fields (p_0, T_0, u_0) are prescribed as the ambient conditions. The free-standing plate is initially at rest $(u_p=0\ \text{m/s})$.

Two types of blast waves are studied in this paper. The uniform incident blast wave can be written as

$$p_i(t) = p_u \tag{3}$$

where p_u is a constant overpressure of the incident blast wave. The second type simulates a typical exponential blast wave, which consists of an abrupt pressure increase followed by slow decay of pressure. There is usually a minor negative phase at the tail end of the blast wave. Neglecting the negative phase, the exponential incident blast wave can be approximated by an exponential profile

$$p_i(t) = p_{is} e^{-t/t_i} \tag{4}$$

where p_{is} is the peak overpressure of the incident blast wave that is at a stand-off distance d_i from the free-standing plate and t_i is the decay time constant. This exponential profile does not correspond to real blast wave propagation but to an approximation that is used for initialization. The density and velocity of both types of incident blast waves are related to the pressure through the classical Rankine–Hugoniot relations

$$\rho_i(t) = \rho_0 \frac{(\gamma+1)p_i(t) + 2\gamma p_0}{(\gamma-1)p_i(t) + 2\gamma p_0}$$

$$u_i(t) = \sqrt{\frac{2}{\gamma p_0}} \frac{a_0 p_i(t)}{\sqrt{(\gamma+1)p_i(t) + 2\gamma p_0}} \tag{5}$$

where a_0 is the speed of sound at ambient conditions.

The above equations serve as the left-hand side boundary conditions for the flow field in front of the plate. On the right-hand side of this flow field, zero gradient boundary conditions are applied to pressure and density. The no-penetration condition is applied to the velocity. These boundary conditions can be written as

$$\frac{\partial p}{\partial x} = 0$$

$$\frac{\partial \rho}{\partial x} = 0$$

$$u = u_p \tag{6}$$

The computational domain for the flow field in front of the plate spans from the initial blast wave to the free-standing plate.

The left-hand side boundary conditions for the flow field at the back of the plate are the same as the right-hand side boundary conditions for the flow field in front of the plate. The right-hand side boundary conditions for the flow field at the back of the plate are given by the ambient conditions and can be written as

$$p = p_0$$

$$\rho = \rho_0$$

$$u = u_0 \tag{7}$$

The initial conditions for the flow fields on both sides of the plate can be described by Eq. (7). The computational domain for the flow field at the back of the plate should be large enough so that the right boundary conditions will not be affected by the induced shock wave.

2.3 Numerical Approach. The Euler equations for the flow fields both in front and at the back of the plate are solved using the van Leer flux vector splitting scheme [13,14] coupled with the monotone upstream-centered scheme for conservation laws (MUSCL) and Runge–Kutta scheme. Because there are sharp gradients in the flow fields for blast wave reflection and shock wave generation, numerical dissipation is needed in the numerical scheme to attenuate numerical errors of small wavelengths. A standard upwind scheme can provide sufficient numerical dissipation for most flow problems that can involve shock waves with large gradients. However, the directions of characteristic velocity should be established before the upwind scheme can be implemented. The van Leer flux vector splitting scheme is applied to split the flux vector F into forward and backward components F^+ and F^- in terms of the local Mach number. F^+ and F^- have characteristic velocities in forward and backward directions, respectively. MUSCL is then used to discretize the spatial derivative of the flux vector. MUSCL is a first-order upwind scheme in the vicinity of the shock and a second-order upwind scheme elsewhere in the flow field. It provides good stability as well as accuracy. A second-order Runge–Kutta explicit scheme is used to discretize the temporal derivatives of the Euler equations.

A second-order Runge–Kutta explicit scheme is used to discretize Newton's second law of motion for the free-standing plate. The detailed numerical scheme and solution algorithm have been described in an earlier work [15].

3 Numerical Validation

To verify the accuracy of the numerical model developed in this study, the flow fields in front and at the back of the plate were simulated separately and compared with results available in the literature.

The following parameters were used in the numerical simulation. The specific heat ratio γ and the gas constant R for air are 1.4 J/kg K and 287 J/kg K, respectively. The density of the steel plate ρ_p is 7800 kg/m^3. The ambient conditions are

$$p_0 = 101.3 \text{ kPa}$$

$$T_0 = 298 \text{ K}$$

$$u_0 = 0 \text{ m/s}$$

3.1 Model Validation: Part I. The simulation of the compressible flow field in front of the free-standing plate, which is subjected to an exponential blast wave, is presented first. The resistance to the plate motion is neglected by assuming a constant atmospheric pressure at the back of the plate. The FSI problem under this assumption was investigated by Kambouchev et al. [1]. Based on the acoustic results for low-intensity waves and the asymptotic limits for extremely light and extremely heavy plates placed within an air environment, they developed a semi-analytical formula to predict the ratio of impulse transmitted to the plate (I_p) to the incident impulse (I_i) for arbitrary blast intensity and plate mass. The impulse transmitted to the plate, defined as $I_p = \int (p_r - p_b) dt$, was used by Kambouchev et al. [1] and shows the net impulse transmitted to the plate. Here, p_r is the overpressure of the reflected blast wave in front of the plate and p_b is the overpressure at the back of the plate. The incident impulse is defined as $I_i = \int p_i dt$, where p_i is the overpressure of the incident blast wave.

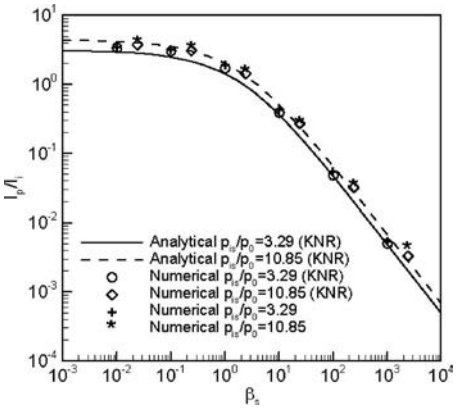

Fig. 2 The ratio of impulse versus compressible FSI parameter for different blast intensities

$$\frac{I_p}{I_i} = \gamma_R \left(\frac{C_R f_R}{\gamma_R} \right)^{\beta_s/(1+\beta_s)} \beta_s^{\beta_s/(1-\beta_s)} \tag{8}$$

where

$$C_R = 2\frac{7 + 4p_{is}/p_0}{7 + p_{is}/p_0} \tag{9}$$

$$f_R = \left(6\frac{p_{is}}{p_0} + 7 \right) \times \sqrt{\frac{(6 + C_R)(p_{is}/p_0) + 7}{(p_{is}/p_0 + 7)[(1 + 6C_R)(p_{is}/p_0) + 7][C_R(p_{is}/p_0) + 7]}} \tag{10}$$

$$\gamma_R = \lim_{\rho_p h_p \to \infty} \frac{I_p}{I_i} = 8 - 42\frac{p_0}{p_{is}} \ln\left(1 + \frac{p_{is}}{7p_0} \right) \tag{11}$$

$$\beta_s = \frac{\rho_{is} U_{is} t_i}{\rho_p h_p} \tag{12}$$

Here, ρ_{is} is the peak density behind the incident shock front, U_{is} is the peak propagation speed of the incident blast wave, and β_s is a nondimensional parameter describing FSI and is inversely proportional to the plate thickness h_p.

The numerical results in this paper are compared with the results of Kambouchev et al. [1] for two different blast intensities of 3.29 and 10.85 and at six different plate thicknesses, as shown in Fig. 2. It can be seen that the numerical results of the present study agree well with the previous results of Kambouchev et al. [1]. The ratio of impulse I_p/I_i decreases with an increase in β_s (decrease in plate thickness). For a plate with large thickness (small β_s), it behaves like a fixed wall. The corresponding ratio of impulse I_p/I_i approaches that of a fixed wall. The reduction in the ratio of impulse I_p/I_i is minimal. For relatively thick plates, there is no significant blast wave mitigation. For thin plates (large β_s), the ratio of impulse I_p/I_i becomes very small for both blast intensities. This means that the blast wave mitigation using a thin plate is very effective.

3.2 Model Validation: Part II. The flow field behind the plate is simulated by including the resistance to the plate motion. A shock wave is induced at the back of the plate due to the plate motion. When the free-standing plate in the left boundary moves with a constant velocity u_p, the overpressure of the shock wave induced by the plate motion is available analytically [16,17],

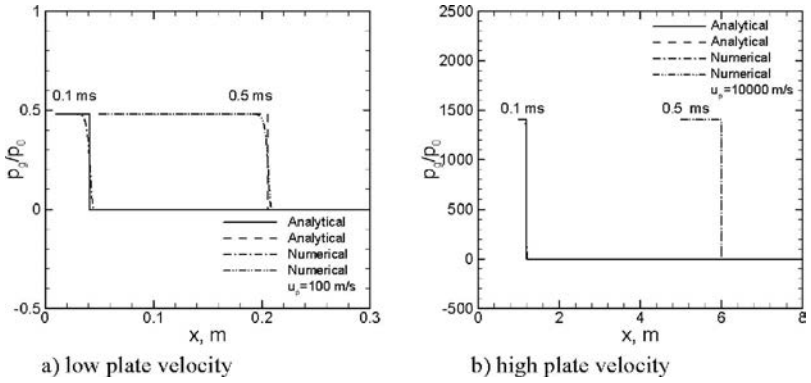

Fig. 3 Numerical and analytical pressure profiles of the induced shock wave behind the plate for (*a*) low and (*b*) high plate velocities at different times

$$u_p = a_0 \left[\frac{(2/\gamma)\dfrac{p_g}{p_0}}{2\gamma\dfrac{p_0}{p_g} + (\gamma+1)} \right]^{1/2} \tag{13}$$

where p_g is the overpressure of the shock wave induced by the plate motion. With a known value of u_p, the overpressure p_g can be determined using Eq. (13).

A plate moving at a constant velocity induces a shock wave, which propagates at a higher speed in the same direction as the plate motion. The pressure profiles of the induced shock wave obtained from the FSI model are compared with the analytical solution at different times of 0.1 ms and 0.5 ms and for plate velocities of 100 m/s and 10,000 m/s. These two plate velocities are used to demonstrate the validity of the numerical model. It can be observed that the numerical results are in good agreement with the analytical solution. The starting point of each curve at different times of 0.1 ms and 0.5 ms indicates the position of the free-standing plate. As shown in Fig. 3, the shock wave strength induced by the plate velocity of 10,000 m/s is many orders of magnitude larger than that induced by the plate velocity of 100 m/s.

3.3 Model Validation: Part III. The flow fields on both sides of the plate are coupled through the receding motion of the plate, which induces a shock wave at the back of the plate. In Ref. [4], Kambouchev derived an analytical solution for acoustic waves interacting with free-standing plates with the presence of a supporting acoustic medium at the back of the plate. The solution is applicable for acoustic waves that are governed by linear wave equations. The net impulse transmitted to the plate is given by [4]

$$\frac{I_p}{I_i} = 2\beta_0^{\frac{\beta_0}{1-\beta_0}} \tag{14}$$

where β_0 is the fluid-structure interaction parameter given by

$$\beta_0 = \frac{(a\overline{\rho} + a_r\overline{\rho_r})t_i}{m_p} \tag{15}$$

Here, a is the speed of sound in the medium in front of the plate whose density is $\overline{\rho}$, a_r is the speed of sound in the medium at the back of the plate whose density is $\overline{\rho_r}$, t_i is the decay time of the exponential incident blast wave, and m_p is the mass of the plate per unit area.

At low blast intensity, the shock wave behaves as an acoustic wave. Numerical results obtained from the present model under such condition can be compared with the analytical solution of Kambouchev [4]. Numerical simulations have been carried out for six different plate thicknesses at an incident acoustic wave, which has a peak intensity of 0.2 and a decay time of 1 ms. The comparison between the numerical results and the analytical solution of Kambouchev [4] is shown in Fig. 4. It can be seen that the numerical results agree well with Kambouchev's analytical solution.

4 Results and Discussion

Numerical simulations of the FSI between a blast wave and a free-standing plate have been carried out. The shock wave induced at the back of the plate is taken into account. In this model, the flow fields on both sides of the plate are coupled through the receding motion of the plate.

4.1 Uniform Blast Wave. As discussed before, the FSI between the receding plate and the induced shock wave at the back of the plate affects the blast wave reflection. The reflection coefficient C is typically defined as the ratio of the reflected blast wave overpressure to the incident blast wave overpressure. The reflection coefficient is analyzed for a free-standing plate subjected to a uniform blast wave. There are two limiting cases of this physical problem. One corresponds to a plate of infinite mass, and the other one corresponds to a plate of infinitesimal mass. For a free-standing plate of infinite mass, the reflection coefficient corresponds to that for a fixed wall, which has been derived previously and can be written as [16]

$$C = \frac{p_r}{p_u} = \frac{(3\gamma-1)p_u/p_0 + 4\gamma}{(\gamma-1)p_u/p_0 + 2\gamma} \tag{16}$$

For air, the range of the reflection coefficient for a plate of infinite mass is

$$2 \le C \le 8$$

The minimum value of 2 corresponds to an acoustic reflection,

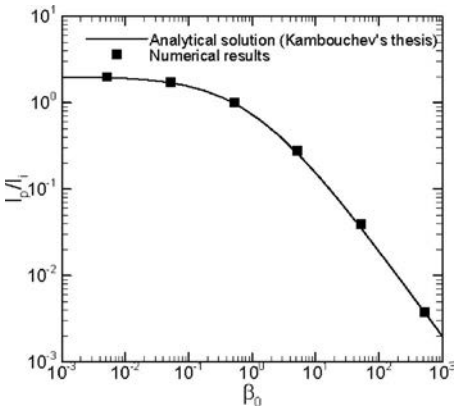

Fig. 4 The ratio of impulse versus FSI parameter for acoustic wave

and the maximum value of 8 corresponds to a strong blast wave reflection.

For a free-standing plate of infinitesimal mass, the inertial effect of the plate is negligible. As the blast wave impacts the plate, the plate accelerates instantaneously to the equilibrium state. This implies that the force exerted by the reflected blast wave in front of the plate should be the same as that exerted by the induced shock wave at the back of the plate.

As discussed in Sec. 3.2, the shock wave strength p_g/p_0 induced by the plate motion is related to the plate velocity u_p through Eq. (13). The reflected blast wave strength is related to the plate velocity u_p through the Rankine–Hugoniot relations. It should be noted that the Rankine–Hugoniot relations for a uniform reflected blast wave are different from the Rankine–Hugoniot relations for a uniform incident blast wave. They can be expressed as

$$\frac{W_r + u_u}{W_r + u_p} = \frac{(\gamma+1)\dfrac{p_r - p_u}{p_u + p_0} + 2\gamma}{(\gamma-1)\dfrac{p_r - p_u}{p_u + p_0} + 2\gamma} \tag{17}$$

where u_u is the fluid velocity behind the incident shock front given by

$$u_u = a_0 \left[\frac{(2/\gamma)\dfrac{p_u}{p_0}}{2\gamma\dfrac{p_0}{p_u} + (\gamma+1)} \right]^{1/2} \tag{18}$$

and W_r is the reflected blast wave speed given by

$$W_r = a_r M_r - u_u \tag{19}$$

The Mach number of the reflected blast wave, M_r, is given by

$$\mathrm{M}_r = \sqrt{\left(\frac{\gamma+1}{2\gamma}\right)\left(\frac{p_r - p_u}{p_u + p_0}\right) + 1} \tag{20}$$

and the speed of sound a_r is related to T_u, the temperature behind the incident shock front, through the equation

$$T_u = T_0 \left[\left(\frac{\gamma-1}{2\gamma}\right)\frac{p_u}{p_0} + 1 \right] \left[\frac{\dfrac{p_u}{p_0} + 1}{\left(\dfrac{\gamma+1}{2\gamma}\right)\dfrac{p_u}{p_0} + 1} \right] \tag{21}$$

For a free-standing plate of infinitesimal mass, p_g is equal to p_r. Combining Eqs. (17)–(21) and Eq. (13) yields a reflection coefficient C of 1.

A free-standing plate initially at rest behaves like a fixed wall. The instant that the blast wave impacts the plate, the reflection coefficient C is expected to approach the value corresponding to a fixed wall. The reflection coefficient C then gradually decreases to its equilibrium value. Numerical simulations have been carried out for free-standing plates of 5 mm and 50 mm thickness at uniform blast intensities of 5 and 50. Figure 5 shows how the reflection coefficient C varies with time. For a fixed wall, the reflection coefficients C for uniform blast wave with blast intensities of 5 and 50 are 4.5 and 7.2, respectively. As shown in Fig. 5, at the instant that the blast wave impacts the plate, the reflection coefficients of free-standing plates approach 4.5 and 7.2 for uniform blast intensities of 5 and 50, respectively. The reflection coefficient gradually decreases with time to its equilibrium value. The equilibrium value for the thinner plate is lower than that for the thicker plate due to the FSI between the blast wave and the plate.

To study how the equilibrium value of reflection coefficient C varies with uniform blast intensities, numerical simulations of the FSI have been carried out for four different plate thicknesses: infinite thickness, 50 mm, 15 mm, and 5 mm. Figure 6 shows the

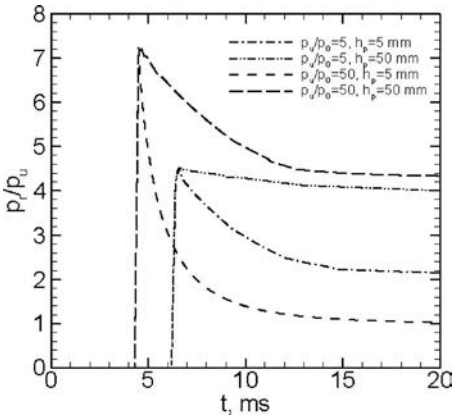

Fig. 5 The reflection coefficient p_r/p_u as a function of time t

equilibrium value of reflection coefficient C for all simulated plate thicknesses at different uniform incident blast intensities. In Fig. 6, the numerical results for a plate of infinite mass are compared with the analytical solution that corresponds to this limiting case. It can be seen that the numerical results for an infinite plate thickness agree well with the analytical results for a fixed wall. The reflection coefficient increases from 2 to 8 with the increase of incident blast intensity. For a small incident blast intensity, all free-standing plates are relatively heavy to the incident blast wave. Therefore, the reflection coefficient for all free-standing plates approaches asymptotically that of a fixed wall. Figure 6 also shows that as the incident blast intensity increases, the reflection coefficient deviates from that of the fixed wall gradually due to the FSI. The inception of the deviation for a thinner plate starts earlier than that for a thicker plate. There is a critical transition point for a particular plate thickness. When the incident blast intensity is greater than the critical transition value, the reflection coefficient starts to decrease. It indicates that the FSI plays a more important role for large blast intensities. As the blast intensity increases further, the reflection coefficient of the free-standing plate of finite mass gradually approaches to that of a plate of infinitesimal mass. As shown in Fig. 6(*a*), the reflection coefficient for the 5 mm thick plate approaches 1 asymptotically when the blast intensity exceeds 30. The reflection coefficients for plates of 15 mm and 50 mm approach 1 as the blast intensity continues to increase (see Fig. 6(*b*)). It should be noted that the reflection coefficient C can never be less than 1.

4.2 Exponential Blast Wave. Numerical simulations of an exponential blast wave interacting with a free-standing plate have been conducted for different blast intensities and plate thicknesses. Because both the incident pressure and reflected pressure vary with time for the exponential blast wave, the reflection coefficient as defined in Sec. 4.1 is not directly applicable to the exponential blast wave. Therefore, the reflected overpressure p_r and the incident overpressure p_i are integrated over the duration of the blast wave to obtain the impulse transmitted to the plate $I_p = \int p_r dt$ and the incident impulse $I_i = \int p_i dt$. Physically, the ratio of impulse I_p/I_i is the average of the reflection coefficient over time.

As can be seen in the previous paragraph, the transmitted impulse used in this paper is different from the definition used by Kambouchev et al. [1], which considered the net impulse transmitted to the plate, namely, $I_p = \int (p_r - p_b) dt$. The definition in the present study considers the impulse transmitted to the plate by the blast wave and properly represents the damage potential of the blast wave. This definition is more meaningful in analysis of blast wave impact. It can be illustrated by a simple thought experiment. For example, if a soldier is impacted by two comparable blast waves on the front and at the back simultaneously, the soldier will suffer from grave injury or death. The net impulse transmitted to

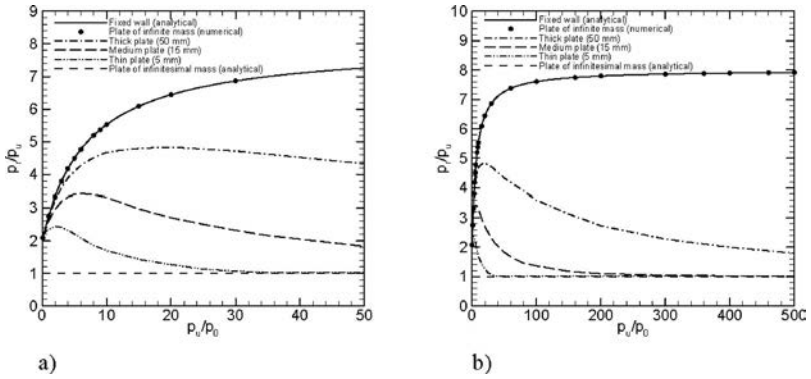

Fig. 6 The reflection coefficient for different plate thicknesses at different uniform incident blast intensities. (*a*) Uniform incident blast intensities of 0–50; (*b*) uniform incident blast intensities of 0–500.

the soldier, using the definition of Kambouchev et al. [1], is negligible. The net transmitted impulse does not provide proper measurement of the damage caused by the blast wave because the damage potential of two blast waves cannot be cancelled. On the other hand, using the definition in this study, both impulses transmitted to the soldier by the blast waves are significant and provide a good measurement of the damage caused by the blast waves.

A blast wave with a peak overpressure of 2 MPa, decay time constant of 0.5 ms, and stand-off distance of 1.6 m is adopted for the numerical simulation. This results in a peak blast intensity of 10.85 right in front of the plate. Approximately the same plate thicknesses (0.000378 mm, 0.00378 mm, 0.0378 mm, 0.378 mm, 3.78 mm, and 37.8 mm) as in Ref. [1] have been simulated. The ratio of impulse transmitted to the plate (I_p) to the incident impulse (I_i) for low blast intensity of 10.85 with resistance at the back of the plate is shown in Fig. 7. For relatively heavy plates, the impact of incident blast wave results in a relatively small receding velocity. This implies that the blast wave mitigation effects of FSI for relatively heavy plates are insignificant. As the thickness of the plate decreases, the receding velocity of the plate increases. The ratio of impulse I_p/I_i decreases. For thicknesses less than about 0.378 mm, the ratio of impulse I_p/I_i reaches a plateau. This is due to the increased resistance at the back of the plate. The impact of the blast wave drives the relatively light plate to very high receding velocity, which induces a strong shock wave at the back of the plate. When the shock wave strength at the back of the plate becomes comparable to the incident blast intensity, the effectiveness of FSI in reducing the blast wave impulse diminishes.

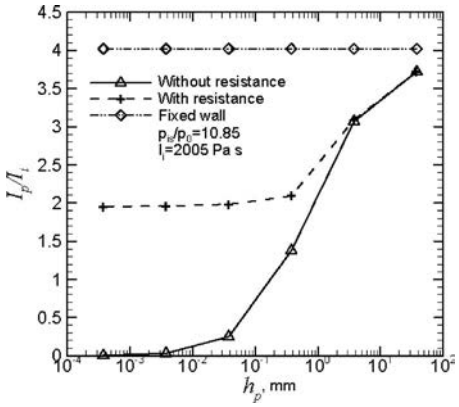

Fig. 7 Comparison between the ratio of impulse I_p/I_i with and without resistance for low blast intensity at different plate thicknesses

The ratio of impulse I_p/I_i was investigated in Ref. [1], where I_p was defined as $I_p=\int(p_r-p_b)dt$. Since the resistance to the plate motion was neglected by assuming a constant atmospheric pressure at the back of the plate in the previous model [1], the overpressure at the back of the plate p_b is 0. Therefore, $I_p=\int(p_r-p_b)dt$ equals $I_p=\int p_r dt$. From the mathematical point of view, the ratio of impulse I_p/I_i defined in this paper is the same as that in Ref. [1]. To investigate whether the resistance at the back of the plate is important, the difference between the numerical results obtained from the two different models is studied. The FSI between a blast wave and a free-standing plate without considering shock wave formation at the back of the plate [1] is also shown in Fig. 7. For relatively heavy plates, the effects of resistance on FSI are not very important. The difference between the ratio of impulse I_p/I_i with and without resistance is very small. As the thickness of the plate decreases, the effects of resistance increase. The difference between the ratio of impulse I_p/I_i with and without resistance becomes significant. While the previous model [1] predicts that it is possible to achieve 100% reduction with a light free-standing plate by neglecting the resistance at the back of the plate, the ratio of impulse I_p/I_i is limited by the resistance at the back of the plate to around 2 for a blast intensity of 10.85. This agrees with the results obtained in Sec. 4.1. It can be seen from Fig. 6 that the reflection coefficient of a free-standing plate can never be less than 1. Since the ratio of impulse transmitted to the plate to the incident impulse I_p/I_i is the average reflection coefficient C, the ratio of impulse I_p/I_i is expected to be always larger than 1. Hence, the previous model [1] significantly overpredicts the effectiveness of FSI in reducing the blast wave impact. For this low blast intensity, the range of small plate thicknesses where the two physical models differ in blast wave mitigation is of limited practical value. However, the difference becomes important for more realistic conditions presented in Figs. 8 and 9.

Results for a blast intensity of 100 are presented in Fig. 8. A blast wave with a peak overpressure of 16 MPa, decay time constant of 0.5 ms, and stand-off distance of 3.2 m is adopted. These parameters result in a peak blast intensity of 100 right in front of the plate. Five different plate thicknesses ranging from 0.00378 mm to 37.8 mm have been simulated. The FSI between a blast wave and a free-standing plate for a blast intensity of 100 behaves very much similar to the blast intensity of 10.85. It is found that the ratio of impulse I_p/I_i reaches a limit of 3.6 for thin plates. The effectiveness of FSI in blast wave mitigation decreases with the increased blast intensity.

Additional simulations are conducted with a blast intensity of 1000. This is achieved by placing a blast wave with a peak overpressure of 150 MPa and decay time constant of 0.5 ms at a stand-off distance of 9.6 m. Four different plate thicknesses rang-

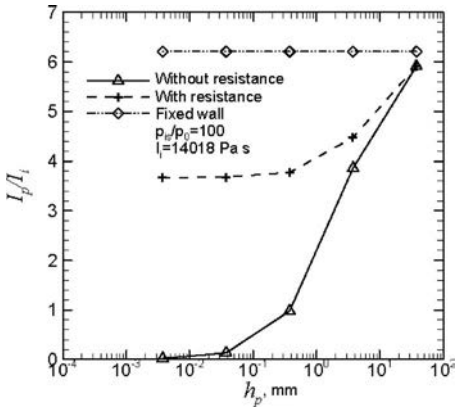

Fig. 8 Comparison between the ratio of impulse I_p/I_i with and without resistance for higher blast intensity at different plate thicknesses

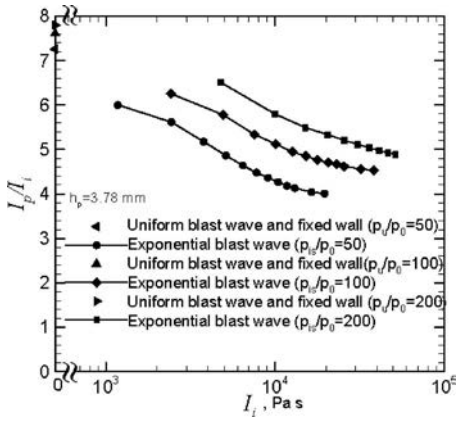

Fig. 10 The ratio of impulse I_p/I_i as a function of incident impulse I_i

ing from 0.0378 mm to 37.8 mm have been simulated. For this blast wave, the ratio of impulse I_p/I_i reaches a limit of 5.4 for thin plates. The difference between the ratio of impulse I_p/I_i with and without resistance becomes 100% for plate thickness of 3.78 mm. As the blast intensity reaches 1000, the relatively thick plate of 3.78 mm is relatively light for the blast wave. Therefore, the resistance at the back of the plate significantly affects the FSI. Neglecting the resistance causes large error in predicting the ratio of impulse I_p/I_i.

The ratio of impulse I_p/I_i is not only affected by the incident peak blast intensity but also by the incident impulse. For a particular incident peak blast intensity, different decay time constants generate different incident impulses. Simulations of a blast wave interacting with a free-standing plate of 3.78 mm are conducted for different incident impulses. An incident blast wave with a peak overpressure of 8 MPa and decay time constants ranging from 0.1 ms to 1.0 ms is placed at different stand-off distances to obtain a constant peak blast intensity of 50 and decay time constants ranging from 0.14 ms to 1.9 ms right in front of the plate with different incident impulses. For an infinitesimal impulse, the pressure instantaneously decays to below the ambient pressure. Therefore, the impulse is completely transmitted to the free-standing plate before it recedes and the FSI has no effect in reducing the blast wave impulse. Hence, the ratio of transmitted impulse to the incident impulse I_p/I_i for an infinitesimal impulse is the same as that on a fixed wall. For a uniform incident blast wave with blast intensity of 50, the ratio of impulse on a fixed wall is 7.2. The reflection coefficient is identical to the ratio of impulse for a uniform blast wave. Since the reflection coefficient for a fixed wall decreases with the decrease of blast intensity, it can be expected that the ratio of impulse of an exponential blast wave will be less than that of a uniform blast wave. It can be seen from Fig. 10 that the ratio of impulse for an exponential blast wave with infinitesimal impulse is slightly below 7.2. As the incident impulse increases, the free-standing plate will recede at a higher velocity. The FSI between the blast wave and the free-standing plate results in the decrease of transmitted impulse as well as the ratio of impulse.

For incident peak overpressures of 16 MPa and 32 MPa and decay time constants ranging from 0.1 ms to 1.0 ms, different stand-off distances are used to obtain peak blast intensities of 100 and 200 right in front of the free-standing plate, where decay time constants ranges from 0.15 ms to 2.0 ms. The ratio of impulse for peak blast intensities of 100 and 200 behaves the same as that for peak blast intensity of 50. It can be seen from Fig. 10 that increased peak blast intensity results in an increasing ratio of impulse.

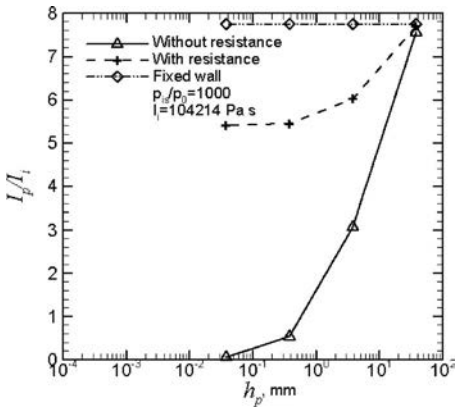

Fig. 9 Comparison between the ratio of impulse I_p/I_i with and without resistance for typical blast wave at different plate thicknesses

5 Conclusions

A numerical model of the FSI between a blast wave and a free-standing plate has been developed. Both the blast wave reflection in front of the plate and the shock wave induced at the back of the plate are considered in the model. The numerical model is validated by comparing it with analytical and numerical results of special cases. Two types of blast wave, uniform and exponential blast wave, are investigated in this paper. For a uniform blast wave, the FSI of a heavy plate resembles the blast wave reflection of a fixed wall. It was shown that the blast wave reflection of a free-standing plate of infinitesimal mass results in an acoustic reflection of a blast wave. The impact on the plate is identical to the incident blast wave pressure. The FSI of a free-standing plate with finite mass falls between these two limiting cases. As the blast intensity increases, the reflection coefficient of the free-standing plate asymptotically approaches 1.

For an exponential blast wave, numerical results show that the effectiveness of FSI in blast wave mitigation increases as the thickness of the plate decreases. However, the effectiveness reaches a plateau after the thickness decreases beyond a critical value. This is due to the increased resistance at the back of the plate. As the thickness of the plate decreases, the impact of the blast wave drives the plate to ever higher receding velocity, which induces a stronger shock wave at the back of the plate. When the shock wave strength at the back of the plate becomes comparable to the incident blast intensity, the effectiveness of FSI in reducing the blast wave impulse diminishes. The model shows that the resistance at the back of the plate plays an important role in the FSI, especially for relatively light plates. Neglecting the resistance

in the previous model [1] significantly overpredicts the effectiveness of FSI. Numerical investigation of the FSI between a blast wave and a free-standing plate also reveals that the ratio of impulse is also highly dependent on the incident blast intensity and impulse. For a particular incident blast intensity, a small decrease in the incident impulse can significantly increase the ratio of impulse. For a constant incident impulse, the increased blast intensity results in an increase of ratio of impulse.

Acknowledgment

Financial support for this study by the U.S. Army Research Office Contract No. W911NF-04-2-0011 is gratefully acknowledged.

Nomenclature

Roman

C = reflection coefficient
F = flux vector
I = impulse per unit area
M = Mach number
R = gas constant
T = temperature
U = solution vector
W = blast wave speed
a = speed of sound
e = internal energy per unit mass
e_t = total energy per unit mass
h = thickness
m = mass
p = pressure
t = time
u = velocity
x = Cartesian coordinate
Δp = pressure difference

Greek

γ = ratio of specific heats
ρ = density

Subscripts

0 = initial condition, ambient condition
b = property at the back of plate
g = property of induced shock wave
i = property of incident blast wave
p = property of plate
r = property of reflected blast wave
s = peak value
u = property of uniform blast wave

References

[1] Kambouchev, N., Noels, L., and Radovitzky, R., 2006, "Nonlinear Compressibility Effects in Fluid-Structure Interaction and Their Implications on the Air-Blast Loading of Structures," J. Appl. Phys., **100**(6), p. 063519.
[2] Kambouchev, N., Noels, L., and Radovitzky, R., 2007, "Numerical Simulation of the Fluid-Structure Interaction Between Air Blast Waves and Free-Standing Plates," Comput. Struct., **85**, pp. 923–931.
[3] Kambouchev, N., Radovitzky, R., and Noels, L., 2007, "Fluid-Structure Interaction Effects in the Dynamic Response of Free-Standing Plates to Uniform Shock Loading," ASME J. Appl. Mech., **74**(5), pp. 1042–1045.
[4] Kambouchev, N., 2007, "Analysis of Blast Mitigation Strategies Exploiting Fluid-Structure Interaction," Ph.D. thesis, Massachusetts Institute of Technology, Cambridge, MA.
[5] Chun, S., Kapoor, H., and Kapania, R. K., 2005, "Nonlinear Fluid-Structure Interaction of Flexible Shelters Under Blast Loading," 46th AIAA/ASME/ASCE/AHS/ASC Structures, Structural Dynamics and Materials Conference, AIAA, Austin, TX, Apr. 18–21, pp. 2005–2176.
[6] Main, J. A., and Gazonas, G. A., 2008, "Uniaxial Crushing of Sandwich Plates Under Air Blast: Influence of Mass Distribution," Int. J. Solids Struct., **45**, pp. 2297–2321.
[7] Espinosa, H. D., Lee, S., and Moldovan, N., 2006, "A Novel Fluid Structure Interaction Experiment to Investigate Deformation of Structural Elements Subjected to Impulsive Loading," Exp. Mech., **46**, pp. 805–824.
[8] Tai, C. H., Teng, J. T., Lo, S. W., and Liu, C. W., 2005, "A Three-Dimensional Numerical Investigation Into the Interaction of Blast Waves With Bomb Shelters," JSME Intl. J., Ser. B, **48**(4), pp. 820–829.
[9] Shi, Y., Hao, H., and Li, Z. X., 2007, "Numerical Simulation of Blast Wave Interaction With Structure Columns," Shock Waves, **17**, pp. 113–133.
[10] Dewey, J. M., and McMillin, D. J., 1981, "An Analysis of the Particle Trajectories in Spherical Blast Waves Reflected From Real and Ideal Surfaces," Can. J. Phys., **59**(10), pp. 1380–1390.
[11] Takayama, K., and Sekiquchi, H., 1981, "Formation and Diffraction of Spherical Shock Waves in a Shock Tube," Rep. Inst. High Speed Mech., Tohoku Univ., **43**, pp. 89–119.
[12] Igra, O., Hu, G., Falcovitz, J., and Heilig, W., 2003, "Blast Wave Reflection From Wedges," ASME J. Fluids Eng., **125**(3), pp. 510–519.
[13] Anderson, W. K., Thomas, J. L., and Van Leer, B., 1986, "Comparison of Finite Volume Flux Vector Splitting for the Euler Equations," AIAA J., **24**(9), pp. 1453–1460.
[14] van Leer, B., 1982, "Flux-Vector Splitting for the Euler Equations," Lect. Notes Phys., **170**, pp. 507–512.
[15] Su, Z., Peng, W., Zhang, Z., Gogos, G., Skaggs, R., and Cheeseman, B., 2008, "Numerical Simulation of a Novel Blast Wave Mitigation Device," Int. J. Impact Eng., **35**(5), pp. 336–346.
[16] Kinney, G. F., and Graham, K. J., 1985, *Explosive Shocks in Air*, 2nd ed., Springer-Verlag, New York, Chap. 5.
[17] Anderson, J. D., 2003, *Modern Compressible Flow: With Historical Perspective*, 3rd ed., McGraw-Hill, New York, Chap. 7.

NO. OF COPIES	ORGANIZATION
1 (PDF)	DEFENSE TECHNICAL INFORMATION CTR DTIC OCA
1 (PDF)	DIRECTOR US ARMY RESEARCH LAB RDRL CIO LL
1 (PDF)	DIRECTOR US ARMY RESEARCH LAB IMAL HRA MAIL & RECORDS MGMT
1 (PDF)	GOVT PRINTG OFC A MALHOTRA

NO. OF COPIES	ORGANIZATION

NO. OF COPIES	ORGANIZATION
1 (PDF)	NSF S MCKNIGHT
2 (PDFS)	DARPA W COBLENZ J GOLDWASSER
1 (PDF)	US AIR FORCE RSRCH LAB K VANDEN
1 (PDF)	US ARMY ARDEC E BAKER
3 (PDFS)	US ARMY RSRCH OFC S MATHAUHDU L RUSSELL JR D STEPP
1 (PDF)	US ARMY TARDEC D TEMPLETON
3 (PDFS)	JOHNS HOPKINS UNIV L BRADY N DAPHALAPURKAR K T RAMESH
1 (PDF)	UNIV OF MISSISSIPPI A M RAJENDRAN
1 (PDF)	UNIV OF SAN DIEGO A VELO
2 (PDFS)	SRI D CURRAN D SHOCKEY
1 (PDF)	PURDUE UNIV W CHEN
1 (PDF)	NYU-POLY S BLESS
1 (PDF)	LOUISIANA STATE UNIV R LIPTON
1 (PDF)	PENN STATE F COSTANZO
1 (PDF)	UNIV TEXAS J FOSTER
1 (PDF)	TEXAS A&M UNIV J WALTON

NO. OF COPIES	ORGANIZATION
	ABERDEEN PROVING GROUND
85 (PDFS)	DIR USARL RDRL WM B FORCH S KARNA P PLOSTINS P BAKER RDRL WML J NEWILL M ZOLTOSKI RDRL WML B I BATYREV S IZVYEKOV B RICE R PESCE RODRIGUEZ D TAYLOR N TRIVEDI N WEINGARTEN RDRL WML C S AUBERT M BISS K MCNESBY RDRL WML D P CONROY M NUSCA RDRL WML E P WEINACHT RDRL WML F D LYON RDRL WML G M BERMAN W DRYSDALE RDRL WML H D SCHEFFLER S SCHRAML B SCHUSTER RDRL WMM J BEATTY R DOWDING J ZABINSKI RDRL WMM A J TZENG RDRL WMM B T BOGETTI R CARTER B CHEESEMAN C FOUNTZOULAS G GAZONAS D HOPKINS T JENKINS R KARKKAINEN B LOVE P MOY B POWERS C RANDOW

NO. OF COPIES	ORGANIZATION
	T SANO
	R WILDMAN
	C YEN
	J YU
	RDRL WMM C
	J LA SCALA
	RDRL WMM D
	E CHIN
	K CHO
	RDRL WMM E
	M COLE
	J LASALVIA
	P PATEL
	J SANDS
	J SINGH
	J SWAB
	RDRL WMM F
	L KECSKES
	H MAUPIN
	RDRL WML G
	J ANDZELM
	A RAWLETT
	RDRL WMP
	S SCHOENFELD
	RDRL WMP B
	M GREENFIELD
	C HOPPEL
	M SCHEIDLER
	T WEERASOORIYA
	RDRL WMP C
	R BECKER
	S BILYK
	T BJERKE
	D CASEM
	J CLAYTON
	B LEAVY
	M RAFTENBERG
	S SATAPATHY
	S SEGLETES
	RDRL WMP D
	R DONEY
	D KLEPONIS
	J RUNYEON
	B SCOTT
	H MEYER
	M ZELLNER
	RDRL WMP E
	M BURKINS
	RDRL WMP F
	A FRYDMAN
	N GNIAZDOWSKI
	R GUPTA
	RDRL WMP G
	N ELDREDGE
	D KOOKER
	S KUKUCK

INTENTIONALLY LEFT BLANK.